Journal of Sound and Vibration 329 (2010) 3550–3564

Contents lists available at ScienceDirect

Journal of Sound and Vibration

journal homepage: www.elsevier.com/locate/jsvi

Rotating flexible disk under shaft temperature increment

Yong-Chen Pei [a,*], Ling He [b], Ji-Xin Wang [a]

[a] Institute of Mechanical Science and Engineering, Jilin University, Nanling Campus, Changchun 130025, People's Republic of China
[b] College of Automotive Engineering, Jilin University, Nanling Campus, Changchun 130025, People's Republic of China

ARTICLE INFO

Article history:
Received 9 September 2009
Received in revised form
7 March 2010
Accepted 7 March 2010
Handling Editor: H. Ouyang
Available online 1 April 2010

ABSTRACT

A rotating flexible annular thin disk subjected to the temperature increment of the shaft clamping the disk was modeled in this paper. At disk top and bottom surfaces and free outer edge, the heat convection boundaries were assumed. Disk transverse deflection was considered as a function of both disk radial and circumferential coordinates, and temperature distribution was solved along disk thickness and radial directions simultaneously. As a result, the shaft temperature increment causes thermo-elastic instability of some disk modes. Effects of the shaft temperature increment, ratio of disk convective heat transfer coefficient to thermal conductivity, disk thickness, nodal circle and diameter numbers of disk mode on the natural frequencies, thermo-elastic instability and critical angular speed of the disk were discussed.

1. Introduction

Rotating disks are widely used as key components in many structural and machinery applications, such as the computer hard disk drives, CD and DVD drivers, the turbine rotors, the circular saws, the disk brakes and clutches for automobile. In practice, the rotating disks are often heated due to friction, driving motor, and other factors. Thermal stresses are induced in the heated disk, which may cause the variation of disk dynamic responses and even result in the thermo-elastic instability. Therefore, the dynamics of a rotating flexible heated disk is a topic of great interest.

There have been some investigations on this topic. Neglecting the temperature distribution along disk thickness, Nieh and Mote [1] studied the vibration and stability of a thermally stressed rotating annular thin disk with an analytical heat transfer model using experimentally measured temperatures at two disk radii as the input of model computation. Under the same negligibility assumption, Mote and Rahimi [2] merged the thermal stresses induced by an axisymmetric temperature distribution into the disk membrane stresses, and presented a system for real-time control of the transverse vibration of a rotating annular thin disk, based on a thermal stressing technique and dynamic system identification. Ghosh [3] investigated the thermal effect on the transverse vibration of a high speed rotating anisotropic solid thin disk in a steady state heat conduction induced by a temperature increment of the disk center, where the disk stiffness (flexural rigidity) was considered to be negligible, and the disk top and bottom surfaces were assumed as insulated boundaries. In Saniei and Luo [4], the natural frequencies and responses for the thermally induced nonlinear free vibration of heated rotating annular disks were presented analytically through an experimentally obtained radial temperature distribution by using local heat transfer measurement data. For automotive disk brakes or clutches, Krempaszky and Lippmann [5] developed a model to estimate the onset of frictionally excited thermo-elastic instabilities

* Corresponding author.
E-mail address: yongchen_pei@hotmail.com (Y.-C. Pei).

0022-460X/$ - see front matter © 2010 Elsevier Ltd. All rights reserved.
doi:10.1016/j.jsv.2010.03.006

Nomenclature

a	disk outer radius
b	disk inner radius
c_v	specific heat at constant volume
C_T	the term of thermo-elastic coupling
conj(•)	operator for complex conjugate
diag[•]	operator for diagonal matrix
E	Young's modulus
g	centrifugal stress
h	disk thickness
h_T	convective heat transfer coefficient
I_Θ	temperature increment integral
I_n,K_n	the modified Bessel functions
J_n,Y_n	Bessel functions
k	thermal conductivity
m	numbers of nodal circle
n	numbers of nodal diameter
$p_{m,n}$	imaginary part of the eigenvalue ϑ
$q_{m,n}$	real part of the eigenvalue ϑ
r	disk radial direction
s_n	instability coefficient
T	disk temperature distribution
T_D	shaft temperature
T_0	disk initial stress-free temperature, i.e. the ambient temperature
w	disk transverse deflection
$x_{m,n}$	deflection of the disk mode (m,n)
z	disk thickness direction
α_T	coefficient of linear thermal expansion
$\delta_{\bullet,\bullet}$	Dirac delta function
ζ	dimensionless disk rotating angular speed
ζ_{cr}	disk critical angular speed
$\zeta_{cr}^{m,n}$	critical angular speed of the disk mode (m,n)
θ	disk circumferential direction
Θ	disk temperature increment
Θ_D	temperature increment of the shaft
$\Theta_{Dc}^{m,n}$	shaft critical temperature increment
λ	eigenvalue of the quadratic eigenvalue problem
ν	Poisson's ratio
ξ_r,ξ_θ	membrane stress resultants of disk temperature increment
ρ	mass per unit volume of the disk
σ_r,σ_θ	membrane stress resultants of disk rotation
Φ	stress function
ϑ	eigenvalue of the self-adjoint eigenvalue problem
$\vartheta_{m,n}$	eigenvalue ϑ of the disk mode (m,n)
Ψ	disk thermal stress
Ψ_H	the homogenous solution of Ψ
Ψ_N	the non-homogenous solution of Ψ
Ω	disk rotating angular speed
$\Omega_{m,n}$	natural frequency of the disk mode (m,n) for a stationary disk

of annular thin disks under thermal pre-stress by assuming the frictional feedback heat flow in disk thickness direction only and considering that the frictional contact induces a radially linear stationary temperature distribution. Under the assumption that the disk vibration deflection was a function of disk radial coordinate only, Nayfeh and Faris [6] considered the problem of large-amplitude vibrations of a simply supported non-rotating solid disk subjected to harmonically varying temperature fields arising from an external heat flux, where the temperature distribution was determined from the radial heat conduction equation subjected to a constant temperature at the disk outer edge. Sun and Tohmyoh [7] considered the thermal conduction along disk thickness only and the insulated disk upper and lower surfaces, established and solved the governing equations of coupled thermo-elastic problems for axisymmetric out-of-plane vibration of non-rotating solid disk. Furthermore, Sun and Tohmyoh [7] used the same assumption of disk deflection in a function of disk radial coordinate as Nayfeh and Faris [6], that is only the axisymmetric disk modes possessing zero nodal diameters were considered in these two works. Using the steady-state heat conduction equation neglecting the temperature distribution along disk thickness and under constant temperatures at inner and outer rims of the disk, Arafat et al. [8] considered the behavior of non-rotating annular disks with clamped–clamped immovable boundary conditions and subjected to axisymmetric in-plane thermal loads. It was found that the thermo-elastic instability for a disk mode possessing non-zero nodal diameters also occurs in the heated disk. Differently from the above works considering the transverse deflection of heated thin disk, the radial displacement was analyzed for thick disks in Kordkheili and Naghdabadi [9], Vivio and Vullo [10] and Vullo and Vivio [11]. A semi-analytical thermo-elasticity solution for hollow and solid rotating axisymmetric disks made of functionally graded materials was presented in Kordkheili and Naghdabadi [9], in which the temperature distribution was solved via the steady state heat transfer equation through the radius direction of the disk subjected to the specified temperatures at inner and outer sides of the disk. Featuring the temperature distribution along disk radius expressed by the polynomial relation, Vivio and Vullo [10] and Vullo and Vivio [11] discussed the analytical procedure for the evaluation of elastic stresses and strains in linear and nonlinear variable thickness rotating disks, either solid or annular, subjected to thermal load, and having a fictitious density variation along the radius.

In this paper, a rotating flexible annular thin disk subjected to the temperature increment of the shaft clamping the disk is developed under the assumption that the disk transverse deflection is a function of both disk radial and circumferential coordinates. At the disk top and bottom surfaces and free outer edge, the heat convection boundaries are assumed. The temperature distribution along the disk thickness and radial directions is considered simultaneously. Natural frequencies, thermo-elastic instability and critical angular speeds of the disk are all determined and discussed.

2. Description of model and boundary conditions

A flexible annular disk clamped at inner radius b and free at outer radius a rotates at a constant angular speed Ω, and the disk thickness h is very small compared with the outer radius. Due to the heat generation of electromagnetic induction in the driving motor and friction in the support bearings, the temperature increment of the shaft (spindle) clamping the disk may be induced inevitably, then disk temperature increases due to the heat conduction between shaft and disk. The temperature increment of the disk is denoted as $\Theta = T - T_0$. From Nayfeh [12] and Awrejcewicz et al. [13], including thermal stresses induced by the temperature increment Θ, the governing equation of the rotating flexible thin disk can be established in the polar coordinates (r,θ) fixed on the ground

$$\rho h\left(\frac{\partial^2 w}{\partial t^2}+2\Omega\frac{\partial^2 w}{\partial t\,\partial\theta}+\Omega^2\frac{\partial^2 w}{\partial\theta^2}\right)+\frac{Eh^3}{12(1-\nu^2)}\nabla^4 w+\rho h\Omega^2 r\left(\frac{r}{2}\nabla^2 w+\frac{\partial w}{\partial r}\right)+\frac{E\alpha_T}{1-\nu}\nabla^2\left(\int_{-h/2}^{h/2}\Theta z\,\mathrm{d}z\right)$$
$$=\frac{\partial^2 w}{\partial r^2}\left(\frac{\partial\Phi}{r\partial r}+\frac{\partial^2\Phi}{r^2\partial\theta^2}\right)+\left(\frac{\partial w}{r\partial r}+\frac{\partial^2 w}{r^2\partial\theta^2}\right)\frac{\partial^2\Phi}{\partial r^2}-2\left(\frac{\partial^2 w}{r\partial r\,\partial\theta}-\frac{\partial w}{r^2\partial\theta}\right)\left(\frac{\partial^2\Phi}{r\partial r\,\partial\theta}-\frac{\partial\Phi}{r^2\partial\theta}\right) \tag{1}$$

where $\nabla^4=\nabla^2\nabla^2$ is a biharmonic differential operator, $\nabla^2=(\partial^2/\partial r^2)+(\partial/r\,\partial r)+(\partial^2/r^2\,\partial\theta^2)$.

The boundary conditions of transverse deflection w at the clamped edge $r=b$ of the disk are

$$w|_{r=b}=0,\quad \partial w/\partial r|_{r=b}=0 \tag{2}$$

Since the bending moment and shear force in the disk vanish at the free edge $r=a$, the boundary conditions are

$$\left[\frac{\partial^2 w}{\partial r^2}+\nu\left(\frac{\partial w}{r\partial r}+\frac{\partial^2 w}{r^2\partial\theta^2}\right)+\frac{12(1+\nu)\alpha_T}{h^3}\left(\int_{-h/2}^{h/2}\Theta z\,\mathrm{d}z\right)\right]\Bigg|_{r=a}=0,$$
$$\left[\frac{\partial}{\partial r}(\nabla^2 w)+\frac{1-\nu}{r^2}\frac{\partial^2}{\partial\theta^2}\left(\frac{\partial w}{\partial r}-\frac{w}{r}\right)+\frac{12(1+\nu)\alpha_T}{h^3}\frac{\partial}{\partial r}\left(\int_{-h/2}^{h/2}\Theta z\,\mathrm{d}z\right)\right]\Bigg|_{r=a}=0 \tag{3}$$

From Nayfeh [12], Nowinski [14] and Awrejcewicz et al. [13], the equation of disk deformation continuity can be modeled as

$$\nabla^4\Phi=2(1-\nu)\rho h\Omega^2-E\alpha_T\nabla^2\left(\int_{-h/2}^{h/2}\Theta\,\mathrm{d}z\right) \tag{4}$$

At the clamped edge $r=b$ and free edge $r=a$, the boundary conditions of the stress function Φ can be written as

$$\left[\frac{\partial^2\Phi}{\partial r^2}-\nu\left(\frac{\partial\Phi}{r\partial r}+\frac{\partial^2\Phi}{r^2\partial\theta^2}\right)-\frac{1}{2}(1-\nu)\rho h\Omega^2 r^2+E\alpha_T\left(\int_{-h/2}^{h/2}\Theta\,\mathrm{d}z\right)\right]\Bigg|_{r=b}=0,$$
$$\left[\frac{\partial}{\partial r}(\nabla^2\Phi)+\frac{1+\nu}{r^2}\frac{\partial^2}{\partial\theta^2}\left(\frac{\partial\Phi}{\partial r}-\frac{\Phi}{r}\right)-(1-\nu)\rho h\Omega^2 r+E\alpha_T\frac{\partial}{\partial r}\left(\int_{-h/2}^{h/2}\Theta\,\mathrm{d}z\right)\right]\Bigg|_{r=b}=0 \tag{5}$$

$$\left(\frac{\partial\Phi}{\partial r}+\frac{1}{r}\frac{\partial^2\Phi}{\partial\theta^2}-\frac{1}{2}\rho h\Omega^2 r^3\right)\Bigg|_{r=a}=0,\quad \left(\frac{\partial^2\Phi}{\partial r\,\partial\theta}-\frac{1}{r}\frac{\partial\Phi}{\partial\theta}\right)\Bigg|_{r=a}=0 \tag{6}$$

From Cho and Ahn [15] and Sun and Tohmyoh [7], the governing equation of disk heat conduction can be stated as

$$\rho c_v\left(\frac{\partial\Theta}{\partial t}+\Omega\frac{\partial\Theta}{\partial\theta}\right)+C_T=k\left(\nabla^2\Theta+\frac{\partial^2\Theta}{\partial z^2}\right) \tag{7}$$

where $C_T=E\alpha_T T_0(2\nu-1)^{-1}z[\partial(\nabla^2 w)/\partial t+\Omega\partial(\nabla^2 w)/\partial\theta]$.

The shaft temperature is specified as a constant T_D at the clamped edge $r=b$ of the disk, and then the boundary condition is

$$\Theta|_{r=b}=\Theta_D \tag{8}$$

where $\Theta_D=T_D-T_0$.

At the free edge $r=a$ and the top $z=h/2$ and bottom $z=-h/2$ surfaces of disk, the convection boundary conditions are assumed

$$\left(h_T\Theta+k\frac{\partial\Theta}{\partial r}\right)\Bigg|_{r=a}=0 \tag{9}$$

$$\left(h_T\Theta+k\frac{\partial\Theta}{\partial z}\right)\Bigg|_{z=h/2}=0,\quad \left(h_T\Theta-k\frac{\partial\Theta}{\partial z}\right)\Bigg|_{z=-h/2}=0 \tag{10}$$

3. Solution procedure of the temperature field

As indicated in Refs. [6,8,13–15], the thermo-elastic coupling term C_T in Eq. (7) is negligible for the thin disk. Since the disk and its boundary conditions are all axisymmetric, the temperature increment Θ is independent of the disk circumferential coordinate θ. Then for the disk in steady state heat conduction, the heat conduction equation Eq. (7) reduces to

$$\frac{\partial^2\Theta}{\partial r^2}+\frac{\partial\Theta}{r\,\partial r}+\frac{\partial^2\Theta}{\partial z^2}=0 \tag{11}$$

From Appendix A, the temperature increment $\Theta(r,z)$ can be obtained as

$$\Theta(r,z)=\Theta_D\sum_{s=1}^{\infty}\overline{R}_s(r)\cos(\omega_s z) \tag{12}$$

where $\overline{R}_s(r)=\beta_s[\varepsilon_s^b \mathrm{I}_0(\omega_s r)-\varepsilon_s^a \mathrm{K}_0(\omega_s r)]/[\varepsilon_s^b \mathrm{I}_0(\omega_s b)-\varepsilon_s^a \mathrm{K}_0(\omega_s b)]$, and $\nabla^2\overline{R}_s=\overline{R}_s''+r^{-1}\overline{R}_s'=\omega_s^2\overline{R}_s$.

Furthermore, integrating $\Theta(r,z)$ along disk thickness yields a temperature increment integral

$$I_\Theta(r)=\int_{-h/2}^{h/2}\Theta\,\mathrm{d}z=\Theta_D\sum_{s=1}^{\infty}2\omega_s^{-1}\overline{R}_s(r)\sin(\omega_s h/2) \tag{13}$$

where $I_\Theta(b)=\Theta_D h$.

Nevertheless, as indicated in Appendix A, the symmetry condition $\Theta(r,-z)=\Theta(r,z)$ always results in

$$\int_{-h/2}^{h/2}\Theta z\,\mathrm{d}z=0 \tag{14}$$

4. Solution procedure of the stress function

From Nayfeh [12], the stress function Φ in Eq. (4) can be expressed as

$$\Phi=g(r)+\Psi(r,\theta,t) \tag{15}$$

With Eq. (15), Eqs. (4)–(6) can be rewritten as

$$\nabla^4\Psi=-E\alpha_T\nabla^2 I_\Theta$$
$$\left[\frac{\partial^2\Psi}{\partial r^2}-\nu\left(\frac{1}{r}\frac{\partial\Psi}{\partial r}+\frac{1}{r^2}\frac{\partial^2\Psi}{\partial\theta^2}\right)+E\alpha_T I_\Theta\right]\Bigg|_{r=b}=0 \tag{16}$$

$$\left[\frac{\partial}{\partial r}(\nabla^2\Psi)+\frac{1+\nu}{r^2}\frac{\partial^2}{\partial\theta^2}\left(\frac{\partial\Psi}{\partial r}-\frac{\Psi}{r}\right)+E\alpha_T\frac{\partial I_\Theta}{\partial r}\right]\Bigg|_{r=b}=0 \tag{17}$$

$$\left(\frac{\partial\Psi}{\partial r}+\frac{1}{r}\frac{\partial^2\Psi}{\partial\theta^2}\right)\Bigg|_{r=a}=0,\quad \left(\frac{\partial^2\Psi}{\partial r\,\partial\theta}-\frac{1}{r}\frac{\partial\Psi}{\partial\theta}\right)\Bigg|_{r=a}=0 \tag{18}$$

Solution of thermal stress Ψ can be expressed as the summation of a homogenous solution and a non-homogenous one

$$\Psi=\Psi_H+\Psi_N \tag{19}$$

Appendices B and C present the formula derivations of Ψ_H and Ψ_N, respectively. As a result, Ψ can be written as

$$\Psi=-E\alpha_T\Theta_D Q(r) \tag{20}$$

where

$$Q(r)=\sum_{s=1}^{\infty}2\sin(\omega_s h/2)\left(\begin{bmatrix}1\\ r^2\\ \ln r\\ r^2\ln r\end{bmatrix}^{\mathrm{T}}\begin{bmatrix}\mathbf{R}''_0(b)-\nu b^{-1}\mathbf{R}'_0(b)\\ \mathbf{R}'''_0(b)+b^{-1}\mathbf{R}''_0(b)-b^{-2}\mathbf{R}'_0(b)\\ \mathbf{R}'_0(a)\\ \mathbf{R}'_0(a)-a^{-1}\mathbf{R}_0(a)\end{bmatrix}^{-1}\begin{bmatrix}\overline{R}_s(b)/\omega_s\\ \overline{R}_s'(b)/\omega_s\\ 0\\ 0\end{bmatrix}+\sum_{m=0}^{\infty}\omega_s\gamma_{m,0}^{-4}\mathbf{S}_{m,0}(\gamma_{m,0}r)\mathbf{d}_{m,0}\int_b^a\overline{R}_s(r)\mathbf{S}_{m,0}(\gamma_{m,0}r)\mathbf{d}_{m,0}r\,\mathrm{d}r\right)$$

5. Solution procedure of the disk deflection

Substituting Eqs. (14), (15) and (20) into Eq. (1) yields

$$\rho h\left(\frac{\partial^2 w}{\partial t^2}+2\Omega\frac{\partial^2 w}{\partial t\,\partial\theta}+\Omega^2\frac{\partial^2 w}{\partial\theta^2}\right)+\frac{Eh^3}{12(1-\nu^2)}\nabla^4 w-\rho h a^2\Omega^2\left[\frac{1}{r}\frac{\partial}{\partial r}\left(r\sigma_r\frac{\partial w}{\partial r}\right)+\frac{1}{r^2}\frac{\partial}{\partial\theta}\left(\sigma_\theta\frac{\partial w}{\partial\theta}\right)\right]$$
$$+E\alpha_T\Theta_D\left[\frac{1}{r}\frac{\partial}{\partial r}\left(r\xi_r\frac{\partial w}{\partial r}\right)+\frac{1}{r^2}\frac{\partial}{\partial\theta}\left(\xi_\theta\frac{\partial w}{\partial\theta}\right)\right]=0 \tag{21}$$

where σ_r and σ_θ are the radial and circumferential membrane stress resultants of disk rotation in Nayfeh [12], $\xi_r=Q'/r$ and $\xi_\theta=Q''$ are the ones of disk temperature increment.

The boundary conditions Eq. (3) reduce to

$$\left[\frac{\partial^2 w}{\partial r^2}+\nu\left(\frac{\partial w}{r\,\partial r}+\frac{\partial^2 w}{r^2\,\partial\theta^2}\right)\right]\Bigg|_{r=a}=0,\quad \left[\frac{\partial}{\partial r}(\nabla^2 w)+\frac{1-\nu}{r^2}\frac{\partial^2}{\partial\theta^2}\left(\frac{\partial w}{\partial r}-\frac{w}{r}\right)\right]\Bigg|_{r=a}=0 \tag{22}$$

Solution of Eq. (21) can be assumed as

$$w=\sum_{m=0}^{\infty}\sum_{n=-\infty}^{\infty}\mathrm{e}^{\mathrm{i}n\theta}\mathbf{B}_{m,n}(\kappa_{m,n}r)\mathbf{c}_{m,n}x_{m,n} \tag{23}$$

where $x_{m,-n}=\mathrm{conj}(x_{m,n})$; $\mathbf{B}_{m,n}(\kappa_{m,n}r)=[\mathrm{J}_n(\kappa_{m,n}r)\quad \mathrm{Y}_n(\kappa_{m,n}r)\quad \mathrm{I}_n(\kappa_{m,n}r)\quad \mathrm{K}_n(\kappa_{m,n}r)]$, $\mathbf{c}_{m,n}=[c_1\quad c_2\quad c_3\quad c_4]^{\mathrm{T}}$, and $\mathbf{B}_{m,n}(\kappa_{m,n}r)\mathbf{c}_{m,n}=\mathbf{B}_{m,-n}(\kappa_{m,-n}r)\mathbf{c}_{m,-n}$; $\kappa_{m,n}$ and $\boldsymbol{c}_{m,n}$ can be determined by the self-adjoint eigenvalue problem corresponding to the boundary conditions Eqs. (2) and (22). Orthonormality condition for the radial mode shape $\mathbf{B}_{m,n}(\kappa_{m,n}r)\mathbf{c}_{m,n}$ is

$$\int_b^a[\mathbf{B}_{m_1,n}(\kappa_{m_1,n}r)\mathbf{c}_{m_1,n}\mathbf{B}_{m_2,n}(\kappa_{m_2,n}r)\mathbf{c}_{m_2,n}]r\,\mathrm{d}r=\delta_{m_1,m_2} \tag{24}$$

From Galerkin's method, substituting Eqs. (20) and (23) into Eq. (21), multiplying Eq. (21) by $\mathrm{e}^{-\mathrm{i}n\theta}\mathbf{B}_{m,n}(\kappa_{m,n}r)\mathbf{c}_{m,n}$ for $m=0,1,\ldots,N_m$ and integrating both sides over the disk area yield an ordinary differential equation for n nodal diameters as

$$\ddot{\mathbf{x}}_n+\mathrm{i}2n\Omega\dot{\mathbf{x}}_n+(\mathbf{S}_n-\alpha_T\Theta_D\mathbf{R}_n+\Omega^2\mathbf{L}_n-n^2\Omega^2\mathbf{I})\mathbf{x}_n=\mathbf{0} \tag{25}$$

where $\mathbf{x}_n=[\cdots\quad x_{m,n}\quad\cdots]^{\mathrm{T}}$, see Appendix D for matrices $\mathbf{I}$, $\mathbf{S}_n$, $\mathbf{L}_n$ and $\mathbf{R}_n$.

The dimensionless variables are related to their dimensional counterparts by the following expressions:

$$\tau=\Omega_{0,0}t,\quad \Omega=\zeta\Omega_{0,0},\quad \mathbf{K}_n=\mathbf{S}_n/\Omega_{0,0}^2,\quad \mathbf{T}_n=\alpha_T\mathbf{R}_n/\Omega_{0,0}^2 \tag{26}$$

where the natural frequency $\Omega_{0,0}$ of disk mode (0,0) can be found in Appendix D.

Eq. (25) becomes

$$\mathrm{d}^2\mathbf{x}_n/\mathrm{d}\tau^2+\mathrm{i}2n\zeta\,\mathrm{d}\mathbf{x}_n/\mathrm{d}\tau+(\mathbf{K}_n-\Theta_D\mathbf{T}_n+\zeta^2\mathbf{L}_n-n^2\zeta^2\mathbf{I})\mathbf{x}_n=\mathbf{0} \tag{27}$$

The homogenous solution of Eq. (27) can be assumed as

$$\mathbf{x}_n=\mathrm{e}^{\lambda\tau}\mathbf{A}_n \tag{28}$$

Substituting Eq. (28) into Eq. (27) yields a quadratic eigenvalue problem

$$[\lambda^2\mathbf{I}+\lambda(\mathrm{i}2n\zeta\mathbf{I})+(\mathbf{K}_n-\Theta_D\mathbf{T}_n+\zeta^2\mathbf{L}_n-n^2\zeta^2\mathbf{I})]\mathbf{A}_n=\mathbf{0} \tag{29}$$

The imaginary part of the eigenvalue λ is the system natural frequency, and the real part can be used to analyze system stability, that is if any eigenvalue λ possesses a positive real part, the corresponding basic solution is unbounded as $t\to\infty$ and the solution is unstable, i.e. thermo-elastic instability.

Let

$$\lambda=\vartheta-\mathrm{i}\,n\zeta \tag{30}$$

Substituting Eq. (30) into Eq. (29) yields a self-adjoint eigenvalue problem

$$[\vartheta^2\mathbf{I}+(\mathbf{K}_n-\Theta_D\mathbf{T}_n+\zeta^2\mathbf{L}_n)]\mathbf{A}_n=\mathbf{0} \tag{31}$$

The natural frequency in the frame fixed on the disk is determined by $p_{m,n}=\mathrm{Im}\,\vartheta_{m,n}$. Let $q_{m,n}=\mathrm{Re}\,\vartheta_{m,n}$, then equilibrium of the flexible disk is unstable when any $\mathrm{Re}\,\lambda=q_{m,n}>0$. Furthermore, an instability coefficient is introduced as

$$s_n=\max_m(q_{m,n}) \tag{32}$$

Therefore, the equilibrium is unstable when $s_n>0$, and the equilibrium is stable when $s_n\le 0$.

When the disk rotates at a critical angular speed, large amplitude transverse vibration occurs [1]. The critical angular speed ζ_{cr} of the disk can be obtained by a self-adjoint eigenvalue problem yielded from Eq. (29) with $\lambda=0$,

$$[(\mathbf{K}_n-\Theta_D\mathbf{T}_n)-\zeta_{cr}^2(n^2\mathbf{I}-\mathbf{L}_n)]\mathbf{A}_n=\mathbf{0} \tag{33}$$

6. Numerical results and discussions

In the following numerical analysis, default parameters of the disk are selected as: $E=200\,\mathrm{GPa}$, $\rho=7840\,\mathrm{kg\,m^{-3}}$, $\nu=0.3$; $\alpha_T=12\times10^{-6}\,\mathrm{K}$, $k=60\,\mathrm{W/(mK)}$, $h_T=60\,\mathrm{W/(m^2\,K)}$, $h_T/k=1\,\mathrm{m^{-1}}$; $a=100\,\mathrm{mm}$, $b=20\,\mathrm{mm}$, $h=1\,\mathrm{mm}$, unless otherwise stated.

The temperature increment Θ_D of the shaft (spindle) clamping the disk causes the disk temperature increment Θ due to the heat conduction between the shaft and the disk. The distribution of disk temperature increment is subjected to the heat convection boundaries at the disk top and bottom surfaces and free outer edge. Determined from the distribution, the radial distributions of the temperature increment integral I_Θ and the thermal stresses Ψ_H, Ψ_N and Ψ are illustrated in Fig. 1(a)–(d), respectively. $I_\Theta(r)/h/\Theta_D$ is employed for the normalization of the temperature increment integral I_Θ in Fig. 1(a), where $I_\Theta(b)/h/\Theta_D=1$, Ψ_H/Θ_D, Ψ_N/Θ_D and Ψ/Θ_D are for those of the thermal stresses in Fig. 1(b)–(d). Since the heat convection on disk surfaces, the temperature increment integral I_Θ drops dramatically along disk radial direction, as shown in Fig. 1(a). The integral I_Θ in the case $h=1\,\mathrm{mm}$ and $h_T/k=1\,\mathrm{m^{-1}}$ is always larger than in the case $h=1\,\mathrm{mm}$ and $h_T/k=3\,\mathrm{m^{-1}}$, whereas smaller than in the case $h=1.2\,\mathrm{mm}$ and $h_T/k=1\,\mathrm{m^{-1}}$. In other words, the decrease of disk thickness h and the increase of the ratio h_T/k of the convective heat transfer coefficient to the thermal conductivity exacerbate the dropping of the disk temperature increment along disk radial direction. As indicated in Eqs. (16)–(18), the disk thermal stress Ψ is deduced by the temperature increment integral I_Θ, and $\Psi=\Psi_H+\Psi_N$, where the homogenous solution Ψ_H is induced by the temperature increment integral I_Θ and its derivative $\partial I_\Theta/\partial r$ at the clamped edge $r=b$, and the non-homogenous one Ψ_N is induced by $\nabla^2 I_\Theta$. As shown in Figs. 1(b) and (c), Ψ_H is positive and decreases consistently towards vanishing along disk radial direction, whereas Ψ_N is negative and increases towards vanishing. As a result, along disk radial direction, the thermal stress Ψ is positive, and firstly increases slightly and arrives at the maximum value $\Psi_{\max}$ around the disk clamping edge, then decreases towards vanishing, as illustrated in Fig. 1(d). The radial position r^* corresponding to the maximum thermal stress $\Psi_{\max}$ can be determined by $\mathrm{d}\Psi/\mathrm{d}r=0$ from Eq. (20). With Eqs. (11) and (13), one has $\nabla^2 I_\Theta=\int_{h/2}^{h/2}\nabla^2\Theta\,\mathrm{d}z=-\int_{h/2}^{h/2}\partial^2\Theta/\partial z^2\,\mathrm{d}z$ in Eqs. (16) and (C.1), thus the distribution of temperature increment Θ along disk thickness

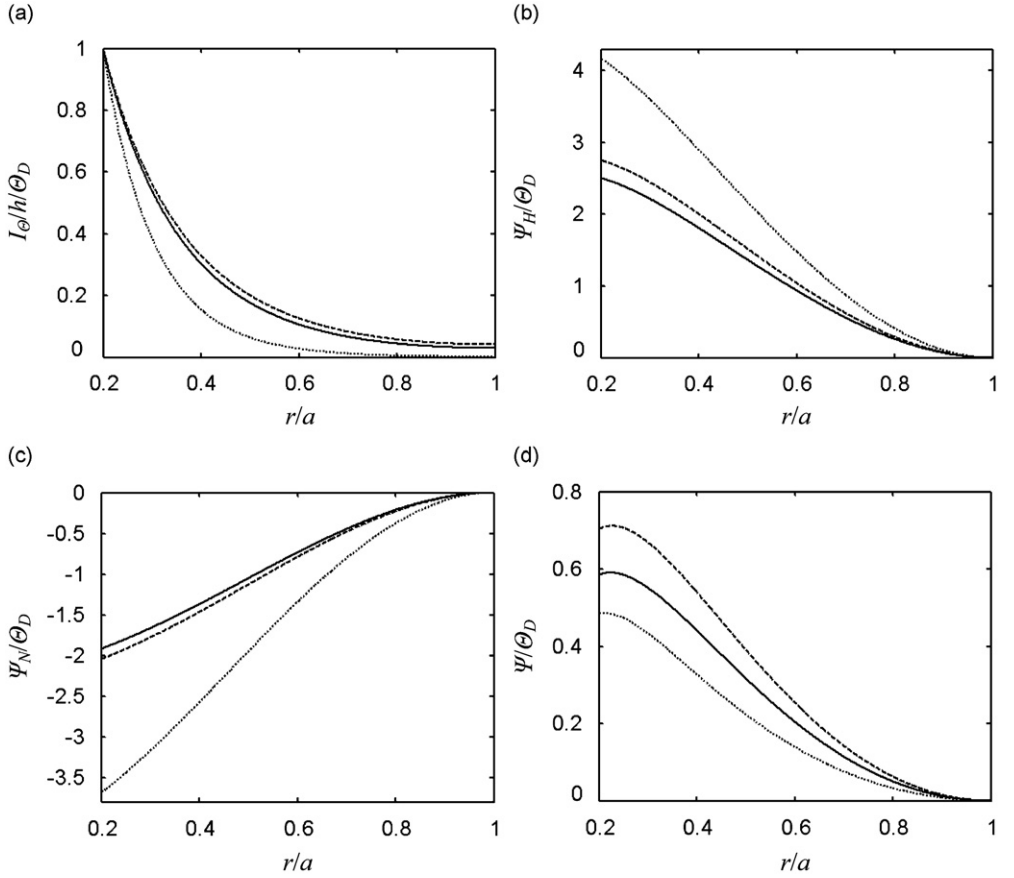

Fig. 1. Radial distributions of the temperature increment integral and the thermal stresses of the disk: (a) the temperature increment integral, (b) the homogenous solution of thermal stress, (c) the non-homogenous solution of thermal stress, and (d) the thermal stress. (——) $h=1\,\mathrm{mm}$, $h_T/k=1\,\mathrm{m^{-1}}$; (· · ·) $h=1\,\mathrm{mm}$, $h_T/k=3\,\mathrm{m^{-1}}$; and (– – –) $h=1.2\,\mathrm{mm}$, $h_T/k=1\,\mathrm{m^{-1}}$.

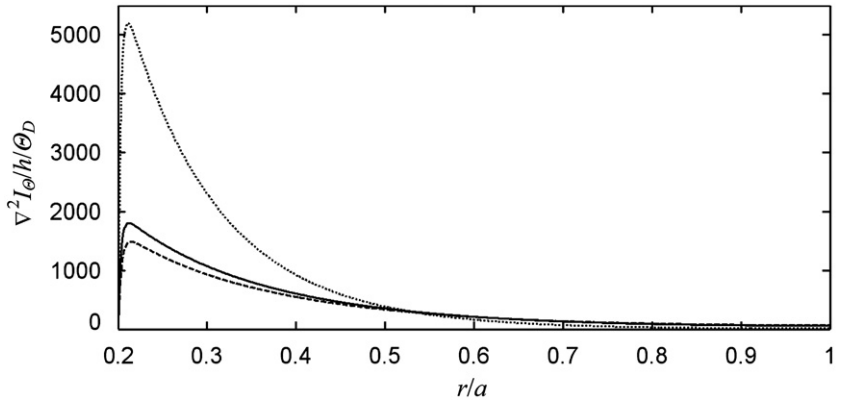

Fig. 2. Radial distribution of $\nabla^2 I_\Theta$. See Fig. 1 for figure key of lines.

$z\in[-h/2,h/2]$ causes Ψ_N. As illustrated in Fig. 2, $\nabla^2 I_\Theta$ is zero at the clamped edge $r=b$ due to the constant temperature increment Θ_D along disk thickness. Along disk radial direction, $\nabla^2 I_\Theta$ firstly increases as a result of the remarkable changes of Θ along disk thickness for the heat convection on disk surfaces, and then decreases gradually because the heat convection becomes weaker with the dropping of Θ. Since the distribution of temperature increment along disk thickness is involved in this paper and Ψ is the combination of the increasing Ψ_N and the decreasing Ψ_H, a maximum thermal stress $\Psi_{\max}$ could occur. Moreover, thermal stress Ψ increases with the increase of disk thickness h and the decrease of ratio h_T/k in Fig. 1(d).

Fig. 3 illustrates effects of the shaft temperature increment Θ_D on the real and imaginary parts of the eigenvalues for a non-rotating disk. The imaginary part $p_{m,n}$ is the natural frequency in the frame fixed on the disk. With the increase of Θ_D, some natural frequencies $p_{m,n}$ decrease, such as $p_{0,0}$ and $p_{0,1}$, but others increase, such as $p_{0,2}$ and $p_{0,3}$. The decreasing $p_{m,n}$ vanishes for large enough Θ_D, such as $p_{0,0}$ and $p_{0,1}$ in Fig. 3(a) and (c) separately. However, $q_{m,n}$ is always zero for Θ_D resulting in non-zero $p_{m,n}$, whereas Θ_D with vanishing $p_{m,n}$ induces non-zero $q_{m,n}$. The minimum value of Θ_D inducing $p_{m,n}=0$ or the maximum one inducing $q_{m,n}=0$ is defined as the shaft critical temperature increment $\Theta_{Dc}^{m,n}$. $p_{m,n}$ and $q_{m,n}$ vanish simultaneously at $\Theta_{Dc}^{m,n}$, as illustrated in Fig. 3(a)–(d). From Eq. (32), any shaft temperature increment larger than $\Theta_{Dc}^{m,n}$ will cause non-zero $q_{m,n}$ and $s_n>0$, then thermo-elastic instability of the heated disk occurs. Furthermore, substituting $\vartheta_{m,n}=q_{m,n}+ip_{m,n}=0$ into Eq. (31) yields a self-adjoint eigenvalue problem $(\mathbf{K}_n-\Theta_D\mathbf{T}_n+\zeta^2\mathbf{L}_n)\mathbf{A}_n=\mathbf{0}$, and $\Theta_{Dc}^{m,n}$ can be determined from it. When $\Theta_D>\Theta_{Dc}^{m,n}$, the value of non-zero $q_{m,n}$ increases consistently for increasing Θ_D, that is thermo-elastic instability becomes more severe. In addition, the disk with larger thickness h holds higher natural frequency $p_{m,n}$, smaller $q_{m,n}$ and larger $\Theta_{Dc}^{m,n}$. Therefore, thick disk is beneficial to suppress the thermo-elastic instability.

As indicated in Fig. 3, the variation of natural frequency $p_{m,n}$ is distinct for the disk modes possessing different nodal circles and diameters, such as $p_{0,1}$, $p_{0,2}$ and $p_{1,2}$. For a non-rotating disk $\zeta=0$, Table 1 presents the increase/decrease trend of $p_{m,n}$ as Θ_D increases for different disk mode (m,n), disk thickness h and the ratio h_T/k. Furthermore, there is a shaft critical temperature increment $\Theta_{Dc}^{m,n}$ only for the disk mode with the decrease trend of $p_{m,n}$. For the disk with $h=1$ mm and $h_T/k=1\,\mathrm{m}^{-1}$ (Case I) or $h=1.2$ mm and $h_T/k=1\,\mathrm{m}^{-1}$ (Case III), the decrease trend happens when $m=0$ and $n\le 1$, $m=1$ and $n\le 3$, $m=2$ and $n\le 6$; but for $h=1$ mm and $h_T/k=3\,\mathrm{m}^{-1}$ (Case II), it happens when $m=0$ and $n\le 1$, $m=1$ and $n\le 2$, $m=2$ and $n\le 4$. Thus, the disk thickness h does not affect the increase/decrease trend of $p_{m,n}$, i.e. the existence of $\Theta_{Dc}^{m,n}$ and thermo-elastic instability for a disk mode (m,n) is not related to the disk thickness. However, the existence extends to the disk modes possessing larger nodal diameters n with the increase of m and the decrease of the ratio h_T/k. Table 1 also indicates value sorting of $p_{m,n}$ for the three Cases I–III. By comparing Case I with Case III, larger disk thickness increases the value of $p_{m,n}$ for any disk mode. Nevertheless, the comparison of Cases I and II indicates that, increasing the ratio h_T/k, the value of $p_{m,n}$ increases when $m=0$ and $n\le 1$, $m=1$ and $n\le 5$, $m=2$ and $n\le 10$ (at least), and the decrease trend of $p_{m,n}$ for disk modes (1,3), (2,5) and (2,6) in Case I becomes the increase trend in Case II. The effects of ratio h_T/k can be interpreted as the decrease of disk thermal stress, as indicated in Fig. 1(d). In addition, since the ratio h_T/k is merged into $\Theta_D\mathbf{T}_n(h_T/k)$ in Eq. (31), the increase of Θ_D promotes the effects of h_T/k on $p_{m,n}$, and there is no effect when $\Theta_D=0$, as illustrated in Fig. 3(a), (c), (e) and (f). Therefore, a larger ratio h_T/k can suppress or even avoid the thermo-elastic instability. Because the natural frequency $p_{m,n}$ and shaft critical temperature increment $\Theta_{Dc}^{m,n}$ of disk mode $m\ge 1$ are much larger than those of $m=0$, as shown in Fig. 3, only the disk modes possessing zero nodal circle $m=0$ are involved in following analysis.

With Eq. (21), potential energies produced by disk membrane stresses of disk rotation and temperature increment can be written as

$$V_\sigma=\frac{1}{2}\int_b^a\int_0^{2\pi}[(\Omega^2\rho h a^2\sigma_r)(\partial w/\partial r)^2+(\Omega^2\rho h a^2\sigma_\theta)(\partial w/\partial\theta/r)^2]r\,\mathrm{d}r\,\mathrm{d}\theta \tag{34}$$

$$V_\xi=\frac{1}{2}\int_b^a\int_0^{2\pi}[(-\Theta_D E\alpha_T\xi_r)(\partial w/\partial r)^2+(-\Theta_D E\alpha_T\xi_\theta)(\partial w/\partial\theta/r)^2]r\,\mathrm{d}r\,\mathrm{d}\theta \tag{35}$$

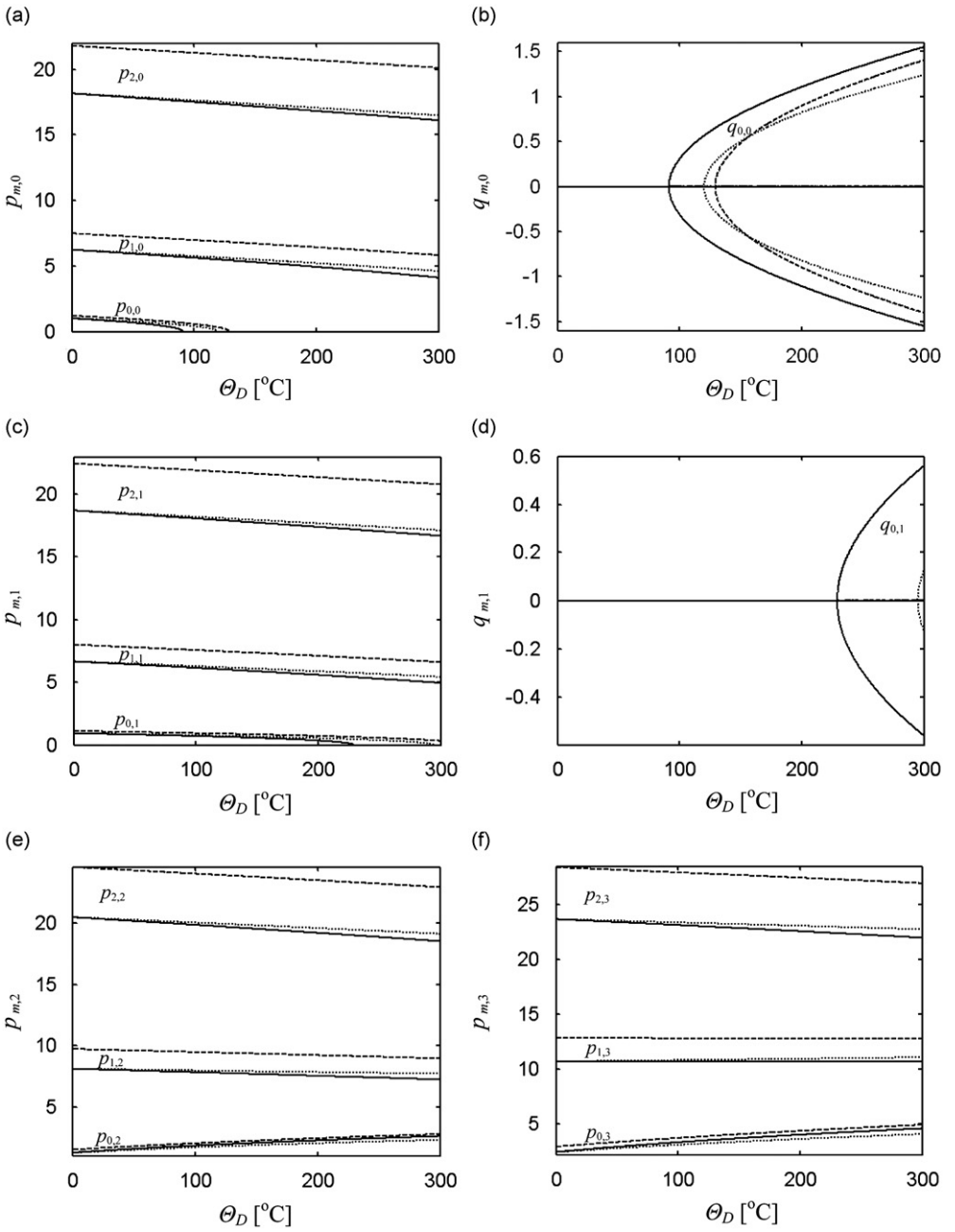

Fig. 3. Effects of the shaft temperature increment on the eigenvalues. ζ=0: (a) and (b) n=0; (c) and (d) n=1; (e) n=2; and (f) n=3. See Fig. 1 for figure key of lines.

where radial distributions of the membrane stress coefficients are illustrated in Fig. 4(a)–(d). From Fig. 4(a), the centrifugal membrane stresses $\Omega^2\rho ha^2\sigma_r$ and $\Omega^2\rho ha^2\sigma_\theta$ due to disk rotation are all always positive, then their mechanical work V_σ is positive, thus they could increase the stiffness of the disk and result in a global positive effect on all natural frequencies [1,2]. The membrane stress resultants ξ_r and ξ_θ in Eq. (21) also can be expressed as $\xi_r=\xi_r^H+\xi_r^N$ and $\xi_\theta=\xi_\theta^H+\xi_\theta^N$ corresponding to the homogenous and non-homogenous solutions of thermal stress $\Psi=\Psi_H+\Psi_N$. Fig. 4(b) and (c) present the radial distributions of homogenous and non-homogenous membrane stresses $-\Theta_D E\alpha_T\xi_r^H$, $-\Theta_D E\alpha_T\xi_\theta^H$ and $-\Theta_D E\alpha_T\xi_r^N$, $-\Theta_D E\alpha_T\xi_\theta^N$ of disk temperature increment, respectively. Along disk radial direction, $-\Theta_D E\alpha_T\xi_r^H$ is always negative, whereas $-\Theta_D E\alpha_T\xi_r^N$ is positive; $-\Theta_D E\alpha_T\xi_\theta^H$ changes from negative to positive, whereas $-\Theta_D E\alpha_T\xi_\theta^N$ from positive to negative. As a result, $(-\Theta_D E\alpha_T\xi_r)=(-\Theta_D E\alpha_T\xi_r^H)+(-\Theta_D E\alpha_T\xi_r^N)$ changes from positive to negative, whereas $(-\Theta_D E\alpha_T\xi_\theta)=(-\Theta_D E\alpha_T\xi_\theta^H)+(-\Theta_D E\alpha_T\xi_\theta^N)$ from negative to positive in Fig. 4(d). Due to the sign change of membrane

Table 1
The increase/decrease trend of natural frequency with the increase of shaft temperature increment for a non-rotating disk.

$p_{m,n}$		n=0	n=1	n=2	n=3	n=4	n=5	n=6	n=7	n=8	n=9	n=10
m=0	I[a]	↘[b],C[c]	↘,C	↗[b],B	↗,B	↗,B	↗,B	↗,B	↗,B	↗,B	↗,B	↗,B
	II[a]	↘,B[c]	↘,B	↗,C	↗,C	↗,C	↗,C	↗,C	↗,C	↗,C	↗,C	↗,C
	III[a]	↘,A[c]	↘,A	↗,A	↗,A	↗,A	↗,A	↗,A	↗,A	↗,A	↗,A	↗,A
m=1	I	↘,C	↘,C	↘,C	↘,C	↗,C	↗,C	↗,B	↗,B	↗,B	↗,B	↗,B
	II	↘,B	↘,B	↘,B	↗,B	↗,B	↗,B	↗,C	↗,C	↗,C	↗,C	↗,C
	III	↘,A	↘,A	↘,A	↘,A	↗,A	↗,A	↗,A	↗,A	↗,A	↗,A	↗,A
m=2	I	↘,C	↘,C	↘,C	↘,C	↘,C	↘,C	↘,C	↗,C	↗,C	↗,C	↗,C
	II	↘,B	↘,B	↘,B	↘,B	↘,B	↗,B	↗,B	↗,B	↗,B	↗,B	↗,B
	III	↘,A	↘,A	↘,A	↘,A	↘,A	↘,A	↘,A	↗,A	↗,A	↗,A	↗,A

[a] I: h=1 mm, h_T/k=1 m^{-1}; II: h=1 mm, h_T/k=3 m^{-1}; III: h=1.2 mm, h_T/k=1 m^{-1}.
[b] ↗: $p_{m,n}$ increases; ↘: $p_{m,n}$ decreases.
[c] Value sorting of $p_{m,n}$ for (I, II, III), A > B > C.

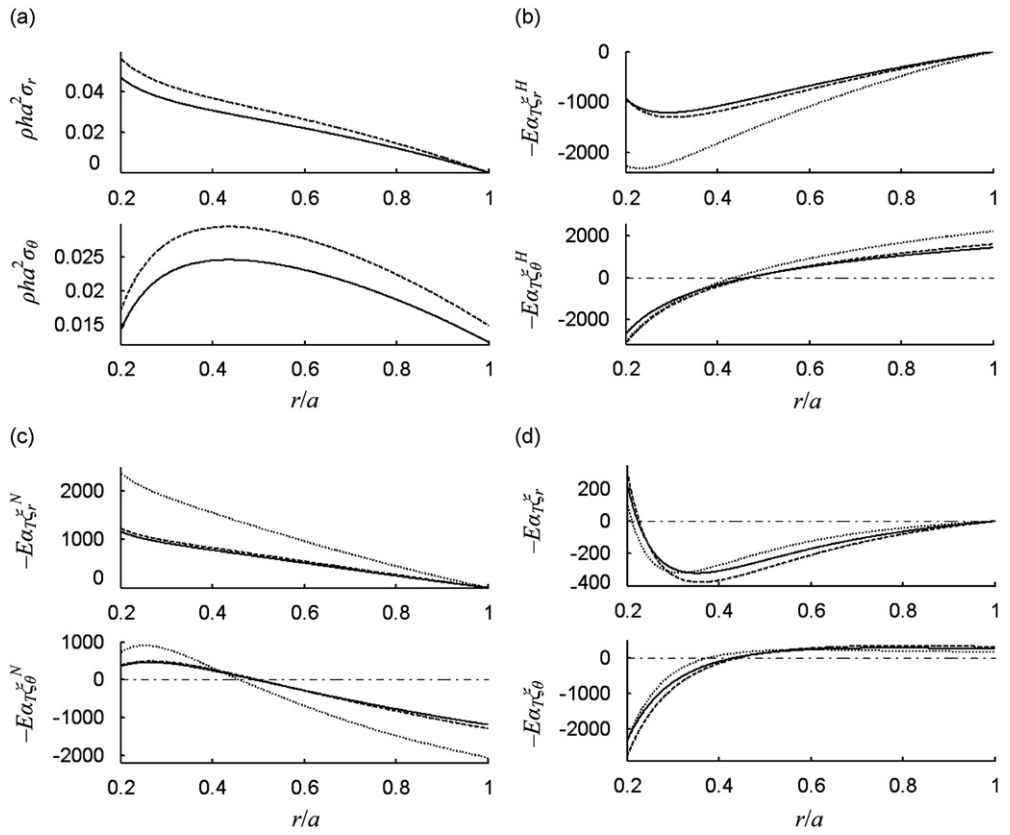

Fig. 4. Radial distributions of disk membrane stress coefficients: (a) the ones of disk rotation, (b) the homogenous ones of disk temperature increment, (c) the non-homogenous ones of disk temperature increment, and (d) the ones of disk temperature increment. See Fig. 1 for figure key of lines.

stresses $-\Theta_D E\alpha_T\xi_r$ and $-\Theta_D E\alpha_T\xi_\theta$ along disk radial direction, they could not have a global negative or positive effect on all natural frequencies depending on the given disk mode (m,n), as indicated in Fig. 3 and Table 1. A similar phenomenon also can be found in Mote and Rahimi [2].

Effects of the disk rotating speed ζ on real and imaginary parts of the eigenvalues are illustrated in Fig. 5. From Fig. 5(a)–(d), large enough Θ_D causes $p_{0,0}$,$p_{0,1}$ vanishing at low speed ζ of disk rotation, and then $p_{0,0}$,$p_{0,1}$ increase when ζ is larger than a critical value ${\zeta_{Sc}}^{0,0}$,${\zeta_{Sc}}^{0,1}$ where $p_{0,0}$,$p_{0,1}$=0 and $q_{0,0}$,$q_{0,1}$=0 simultaneously. Correspondingly, the real parts $q_{0,0}$,$q_{0,1}$ are non-zero when $\zeta \leqslant {\zeta_{Sc}}^{0,0}$,${\zeta_{Sc}}^{0,1}$, and then $q_{0,0}$,$q_{0,1}$ vanish when $\zeta > {\zeta_{Sc}}^{0,0}$,${\zeta_{Sc}}^{0,1}$. Therefore, due to the centrifugal stress $g(r)$ induced by the disk rotation, the larger disk rotating speed ζ can suppress or even avoid the thermo-elastic instability. As shown in Fig. 3(b), (d) and 5(b), (d), the values of non-zero $q_{0,0}$ are much larger than that of $q_{0,1}$, that is the

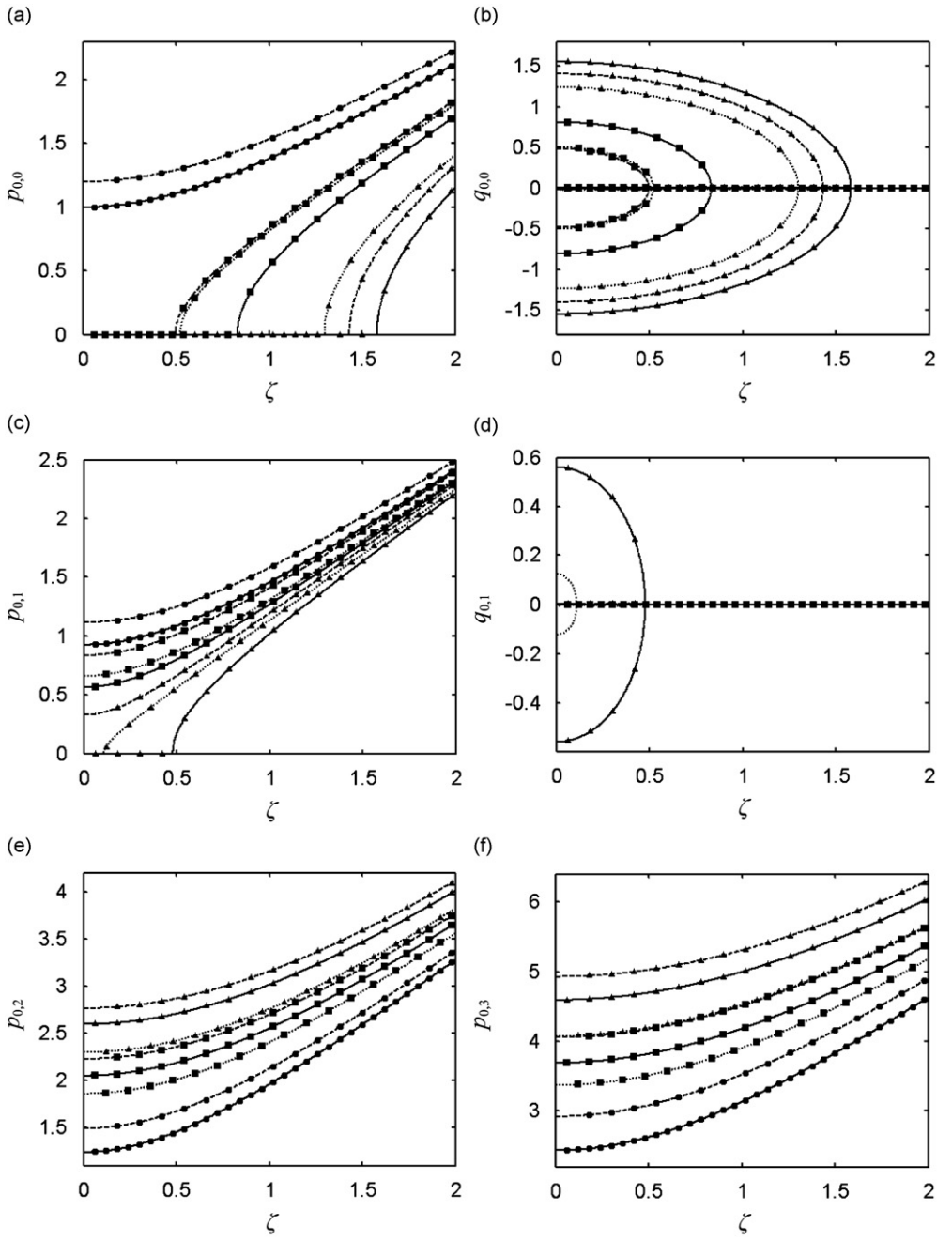

Fig. 5. Effects of the disk rotating speed on the eigenvalues: (a) and (b) m=0, n=0; (c) and (d) m=0, n=1; (e) m=0, n=2; and (f) m=0, n=3. (●) Θ_D=0 °C; (■) Θ_D=150 °C; and (▲) Θ_D=300 °C. See Fig. 1 for figure key of lines.

thermo-elastic instability of disk mode (0,0) is much more dangerous than that of (0,1). However, the natural frequencies $p_{0,2}$,$p_{0,3}$ increase consistently for increasing disk rotating speed ζ, as shown in Fig. 5(e) and (f). As a result, the zero $p_{0,2}$,$p_{0,3}$ and non-zero $q_{0,2}$,$q_{0,3}$ cannot appear, then the thermo-elastic instability is absent for the disk modes (0,2) and (0,3). As illustrated in Fig. 5, with the increase of disk thickness h, $p_{0,0}$,$p_{0,1}$ and $p_{0,2}$,$p_{0,3}$ increase, but $q_{0,0}$,$q_{0,1}$ decrease. Furthermore, the larger ratio h_T/k increases $p_{0,0}$,$p_{0,1}$ and decreases $q_{0,0}$,$q_{0,1}$ and $p_{0,2}$,$p_{0,3}$. Nevertheless, $p_{0,2}$,$p_{0,3}$ cannot vanish, because the shaft temperature increment Θ_D not only determines the performances of h_T/k, i.e. $\Theta_D\mathbf{T}_n(h_T/k)$ in Eq. (31), but also increases $p_{0,2}$,$p_{0,3}$, as indicated in Fig. 3(e) and (f) and Table 1.

From Figs. 3(a)–(d) and 5(a)–(d), the shaft critical temperature increment ${\Theta_{Dc}}^{m,n}$ appears when $\vartheta_{m,n}=q_{m,n}+ip_{m,n}=0$, and then it can be determined by the self-adjoint eigenvalue problem $(\mathbf{K}_n-\Theta_D\mathbf{T}_n+\zeta^2\mathbf{L}_n)\mathbf{A}_n=\mathbf{0}$. ${\Theta_{Dc}}^{m,n}$ varying with the disk rotating speed ζ is illustrated in Fig. 6(a) and (b) for the disk mode (0,0) and (0,1), respectively, i.e. the boundaries of

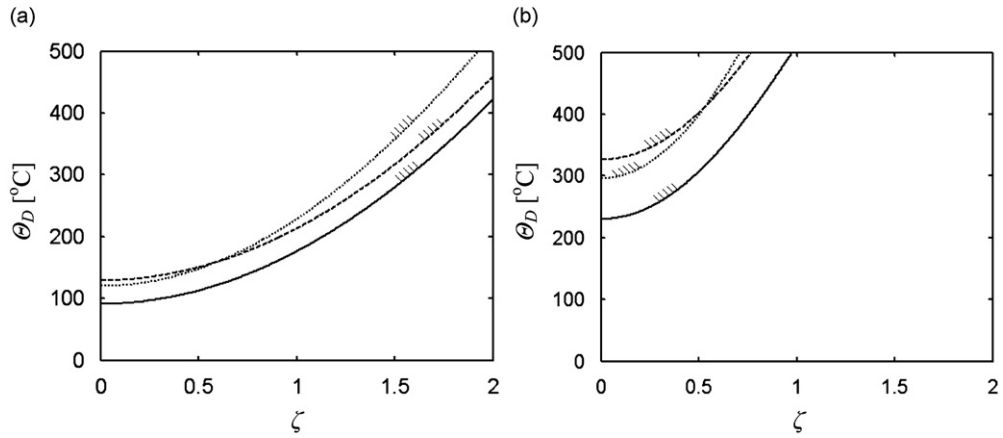

Fig. 6. Parameter boundaries of thermo-elastic instability: (a) m=0, n=0; and (b) m=0, n=1. See Fig. 1 for figure key of lines.

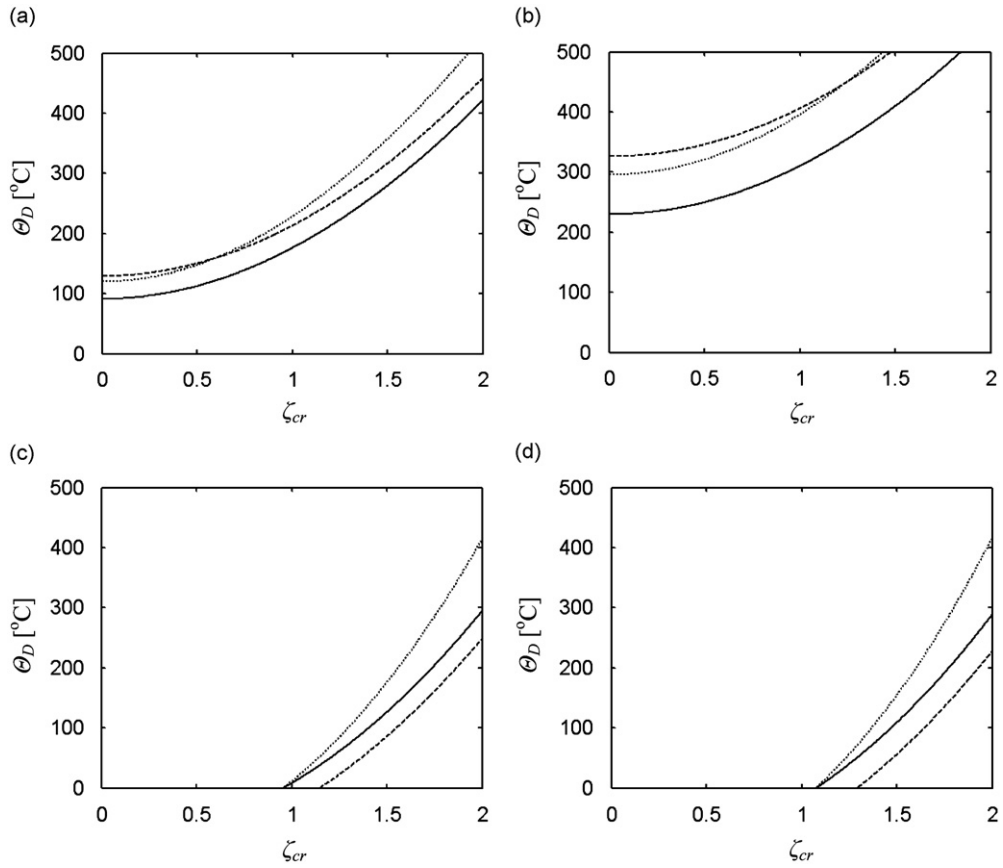

Fig. 7. Effects of the shaft temperature increment on the disk critical angular speed: (a) m=0, n=0; (b) m=0, n=1; (c) m=0, n=2; and (d) m=0, n=3. See Fig. 1 for figure key of lines.

thermo-elastic instability are plotted in the $\zeta-\Theta_D$ parameter plane. The values of ${\Theta_{Dc}}^{0,1}$ are much larger than those of ${\Theta_{Dc}}^{0,0}$, thus the thermo-elastic instability of disk mode (0,0) is more easily induced. Furthermore, ${\Theta_{Dc}}^{0,0}$ and ${\Theta_{Dc}}^{0,1}$ increase consistently with the increase of disk rotating speed ζ, the disk thickness h and ratio h_T/k also increase them, as shown in Fig. 6.

In Fig. 7, the effects of the shaft temperature increment Θ_D on the disk critical angular speed ζ_{cr} are illustrated. From Eqs. (30) and (31), $\lambda_{m,n}$ can be rewritten as $q_{m,n}+\mathrm{i}(p_{m,n}-n\zeta)$. In Eq. (33), the value of ζ_{cr} is determined from Eq. (29) under the condition of $\lambda_{m,n}$=0, i.e. $q_{m,n}$=0 and $p_{m,n}=n\zeta$. Nevertheless, the shaft critical temperature increment ${\Theta_{Dc}}^{m,n}$ appears

when $\vartheta_{m,n}=0$, i.e. $q_{m,n}=0$ and $p_{m,n}=0$, as discussed in the above sections. Therefore, for the disk mode possessing zero nodal diameter ($n=0$) only, which can cause $n\zeta=0$, the boundaries of thermo-elastic instability in Fig. 6(a) are the same lines of the disk critical angular speed ζ_{cr} varying with the shaft temperature increment Θ_D in Fig. 7(a). For disk mode (0,0) and (0,1), one has $n^2\mathbf{I}-\mathbf{L}_n<0$ in Eq. (33) which always causes the absence [16] of critical angular speeds for a rotating free disk without the thermal factor ($\Theta_D=0$), but there is ζ_{cr} if and only if $\mathbf{K}_n-\Theta_D\mathbf{T}_n<0$. Then Eq. (33) can be rewritten as $[(\Theta_D\mathbf{T}_n-\mathbf{K}_n)-\zeta_{cr}^2(\mathbf{L}_n-n^2\mathbf{I})]\mathbf{A}_n=\mathbf{0}$, where Θ_D has a negative effect on $\mathbf{K}_n-\Theta_D\mathbf{T}_n$ and natural frequencies $p_{0,0}$ and $p_{0,1}$ as given in Fig. 3 and Table 1, so that a large enough Θ_D could result a positive effect on $\Theta_D\mathbf{T}_n-\mathbf{K}_n$ and $\zeta_{cr}^{0,0},\zeta_{cr}^{0,1}$, as shown in Figs. 7 (a) and (b). For disk mode (0,2) and (0,3), one has $n^2\mathbf{I}-\mathbf{L}_n>0$, there is ζ_{cr} when $\mathbf{K}_n-\Theta_D\mathbf{T}_n>0$, where Θ_D has a positive effect on $\mathbf{K}_n-\Theta_D\mathbf{T}_n$ and natural frequencies $p_{0,2}$ and $p_{0,3}$ in Fig. 3 and Table 1, thus $\zeta_{cr}^{0,2},\zeta_{cr}^{0,3}$ increases in Fig. 7(c) and (d). Furthermore, there are $\zeta_{cr}^{0,2},\zeta_{cr}^{0,3}$ at $\Theta_D=0$, then $\zeta_{cr}^{0,2},\zeta_{cr}^{0,3}$ increase with the increase of Θ_D, as illustrated in Fig. 7(c) and (d). The larger disk thickness h decreases $\zeta_{cr}^{0,0},\zeta_{cr}^{0,1}$ but increases $\zeta_{cr}^{0,2},\zeta_{cr}^{0,3}$. Nevertheless, $\zeta_{cr}^{0,0},\zeta_{cr}^{0,1}$ and $\zeta_{cr}^{0,2},\zeta_{cr}^{0,3}$ decrease as the ratio h_T/k increases. Therefore, a small ratio h_T/k is beneficial to increase the disk critical angular speed.

7. Conclusions

A rotating flexible annular disk subjected to the temperature increment of the shaft clamping the disk was modeled in this paper. Natural frequencies, thermo-elastic instability and critical angular speed of the disk were determined and discussed. The following conclusions can be drawn:

(1) Disk thermal stress induced by the shaft temperature increment increases for increasing disk thickness and decreasing ratio of disk convective heat transfer coefficient to thermal conductivity.
(2) Thermo-elastic instability of the disk occurs when the natural frequency in the frame fixed on the disk of a disk mode can decrease and vanish with the increase of shaft temperature increment.
(3) The thermo-elastic instability extends to the disk modes possessing larger nodal diameters with the increase of nodal circle number and the decrease of ratio of disk convective heat transfer coefficient to thermal conductivity.
(4) The thermo-elastic instability can be suppressed or avoided by increasing ratio of disk convective heat transfer coefficient to thermal conductivity, disk thickness and rotating angular speed.
(5) Disk critical angular speed increases as ratio of disk convective heat transfer coefficient to thermal conductivity decreases and the shaft temperature increment increases.

Acknowledgments

This work is supported by the Fundamental Research Funds of Jilin University P.R. China (Scientific Frontier and Interdisciplinary Innovation Project) under Grant no. 200903170: Multi-Body Dynamics of Rotating Flexible Disk with Thermo-Elastic Coupling; Jilin Provincial Science & Technology Department: Study on the key technology of disk brake based on multi-field coupling method (20080109). The authors would like to thank Chassis Part Factory, Changchun FAW-Sihuan Automobile Co., Ltd., P.R. China for their help in contributing to the completeness of this paper.

Appendix A. Formula derivations of the temperature increment $\Theta(r,z)$

Using the method of separation variables, the solution of $\Theta(r,z)$ can be assumed as

$$\Theta(r,z)=Z(z)R(r) \tag{A.1}$$

Substituting Eq. (A.1) into Eq. (11) yields $(R''+R'/r)/R=-Z''/Z=\omega^2$, $\omega>0$, thus

$$Z''+\omega^2 Z=0 \tag{A.2}$$

$$R''+r^{-1}R'-\omega^2 R=0 \tag{A.3}$$

Solution of Eq. (A.2) can be expressed as

$$Z=c_1\sin(\omega z)+c_2\cos(\omega z) \tag{A.4}$$

Substituting the solution Eq. (A.4) into Eq. (10) yields a self-adjoint eigenvalue problem

$$\begin{bmatrix} h_T\sin(\omega h/2)+k\omega\cos(\omega h/2) & h_T\cos(\omega h/2)-k\omega\sin(\omega h/2) \\ -h_T\sin(\omega h/2)-k\omega\cos(\omega h/2) & h_T\cos(\omega h/2)-k\omega\sin(\omega h/2) \end{bmatrix}\begin{bmatrix} c_1 \\ c_2 \end{bmatrix}=\mathbf{0} \tag{A.5}$$

When the matrix determinant of Eq. (A.5) vanishes, ω can be determined from

$$\omega_s h+2\tan^{-1}(k\omega_s/h_T)=(2s-1)\pi \ \text{ with } \ c_1=0 \ \text{ and } \ c_2=1 \tag{A.6}$$

$$\omega_s h+2\tan^{-1}(k\omega_s/h_T)=2s\pi \ \text{ with } \ c_1=1 \ \text{ and } \ c_2=0 \tag{A.7}$$

where s=1,2,…. Since the temperature increment Θ_D considered is symmetric with respect to z=0, $\Theta(r,-z)=\Theta(r,z)$ yields c_1=0 in Eq. (A.4), i.e. $Z=c_2\cos(\omega z)$, then ω_s solved from Eq. (A.7) with c_2=0 is meaningless.

Solution of Eq. (A.3) can be expressed as

$$R_s = b_s \mathrm{I}_0(\omega_s r) + d_s \mathrm{K}_0(\omega_s r) \tag{A.8}$$

Substituting Eq. (A.8) into the boundary condition Eq. (9) yields

$$d_s = -\varepsilon_s^a b_s/\varepsilon_s^b \tag{A.9}$$

where ${\varepsilon_s}^a = h_T \mathrm{I}_0(\omega_s a) + \omega_s k \mathrm{I}_1(\omega_s a)$, ${\varepsilon_s}^b = h_T \mathrm{K}_0(\omega_s a) - \omega_s k \mathrm{K}_1(\omega_s a)$.

With Eqs. (A.4) and (A.8), substituting Eq. (A.1) into the boundary condition Eq. (8) yields

$$\Theta(b,z) = \sum_{s=1}^{\infty} \cos(\omega_s z)[\varepsilon_s^b \mathrm{I}_0(\omega_s b) - \varepsilon_s^a \mathrm{K}_0(\omega_s b)] b_s/\varepsilon_s^b = \Theta_D \tag{A.10}$$

where b_s can be solved by the least squares fitting method using $\cos(\omega_s z)$ as the basis function

$$b_s = \frac{\Theta_D \varepsilon_s^b \beta_s}{\varepsilon_s^b \mathrm{I}_0(\omega_s b) - \varepsilon_s^a \mathrm{K}_0(\omega_s b)} \tag{A.11}$$

$$\begin{bmatrix} \vdots \\ \beta_s \\ \vdots \end{bmatrix} = \begin{bmatrix} \ddots & \cdots & \iddots \\ \cdots & \int_{-h/2}^{h/2} \cos(\omega_{s_1} z)\cos(\omega_{s_2} z)\,\mathrm{d}z & \cdots \\ \iddots & \cdots & \ddots \end{bmatrix}^{-1} \begin{bmatrix} \vdots \\ \int_{-h/2}^{h/2} \cos(\omega_s z)\,\mathrm{d}z \\ \vdots \end{bmatrix} \tag{A.12}$$

where s_1, s_2=1,2,….

As a result,

$$\Theta(r,z) = \Theta_D \sum_{s=1}^{\infty} \beta_s \frac{\varepsilon_s^b \mathrm{I}_0(\omega_s r) - \varepsilon_s^a \mathrm{K}_0(\omega_s r)}{\varepsilon_s^b \mathrm{I}_0(\omega_s b) - \varepsilon_s^a \mathrm{K}_0(\omega_s b)} \cos(\omega_s z) \tag{A.13}$$

Appendix B. Formula derivations of the homogenous solution Ψ_H

The homogenous form of Eqs. (16)–(18) can be written as

$$\nabla^4 \Psi_H = 0$$

$$\left[\frac{\partial^2 \Psi_H}{\partial r^2} - \nu\left(\frac{1}{r}\frac{\partial \Psi_H}{\partial r} + \frac{1}{r^2}\frac{\partial^2 \Psi_H}{\partial \theta^2}\right) + E\alpha_T I_\Theta\right]\Bigg|_{r=b} = 0 \tag{B.1}$$

$$\left[\frac{\partial}{\partial r}(\nabla^2 \Psi_H) + \frac{1+\nu}{r^2}\frac{\partial^2}{\partial \theta^2}\left(\frac{\partial \Psi_H}{\partial r} - \frac{\Psi_H}{r}\right) + E\alpha_T \frac{\partial I_\Theta}{\partial r}\right]\Bigg|_{r=b} = 0 \tag{B.2}$$

$$\left(\frac{\partial \Psi_H}{\partial r} + \frac{1}{r}\frac{\partial^2 \Psi_H}{\partial \theta^2}\right)\Bigg|_{r=a} = 0, \quad \left(\frac{\partial^2 \Psi_H}{\partial r\,\partial \theta} - \frac{1}{r}\frac{\partial \Psi_H}{\partial \theta}\right)\Bigg|_{r=a} = 0 \tag{B.3}$$

Solution of Eq. (B.1) can be assumed as

$$\Psi_H = \sum_{n=-\infty}^{\infty} \mathrm{e}^{\mathrm{i}n\theta} \Psi_n^H(r,t) \tag{B.4}$$

Substituting the solution Eq. (B.4) into Eq. (B.1) yields

$${\Psi''''}_n^H + 2r^{-1}{\Psi'''}_n^H - r^{-2}(2n^2+1){\Psi''}_n^H + r^{-3}(2n^2+1){\Psi'}_n^H + r^{-4}(n^2-4)n^2 \Psi_n^H = 0 \tag{B.5}$$

For $n \neq 0$, the solution of ${\Psi_n}^H$ can be expressed as

$$\Psi_n^H = \mathbf{R}_n(r)\mathbf{c}_n^H \tag{B.6}$$

where $\mathbf{c}_n^H = [h_1 \quad h_2 \quad h_3 \quad h_4]^{\mathrm{T}}$ and $\mathbf{R}_n(r) = [r^{-n} \quad r^n \quad r^{2-n} \quad r^{2+n}]$.

Since $I_\Theta(r)$ is not related to the disk circumferential coordinate θ, substituting Eqs. (B.4) and (B.6) into the boundary conditions Eqs. (B.2) and (B.3) yields ${\mathbf{c}_n}^H = \mathbf{0}$.

Specially, when n=0, Eq. (B.5) becomes

$${\Psi''''}_0^H + 2r^{-1}{\Psi'''}_0^H - r^{-2}{\Psi''}_0^H + r^{-3}{\Psi'}_0^H = 0 \tag{B.7}$$

Substituting Eq. (B.4) into the second boundary condition in Eq. (B.3) yields $\mathrm{i}n({\Psi_n}'^H - {\Psi_n}^H/r)|_{r=a} = 0$, but which always vanishes when n=0, then only the solution of ${\Psi_n}'^H$ can be solved from Eq. (B.7) and its other boundary conditions in Eqs. (B.2) and (B.3). However, $({\Psi_n}'^H - {\Psi_n}^H/r)|_{r=a} = 0$ is available to solve ${\Psi_n}^H(\mathbf{c}_n^H)$ for a non-zero n in Eq. (B.6).

Similarly, $(\Psi_0{}'^H - \Psi_0^H/r)|_{r=a}=0$ can be remained to solve Ψ_0^H, and the remaining does not affect the solution of $\Psi_0{}'^H$. Further, solution of Ψ_0^H can be solved as

$$\Psi_0^H = \mathbf{R}_0(r)\mathbf{c}_0^H \tag{B.8}$$

where $\mathbf{c}_0^H=[\,h_1 \quad h_2 \quad h_3 \quad h_4\,]^{\mathrm{T}}$, and $\mathbf{R}_0(r)=[\,1 \quad r^2 \quad \ln r \quad r^2\ln r\,]$.

By substituting Eq. (B.8) into the boundary conditions Eqs. (B.2) and (B.3) with the remaining, $\mathbf{c}_0^H$ can determined as

$$\mathbf{c}_0^H = -E\alpha_T\Theta_D\sum_{s=1}^{\infty}2\sin(\omega_s h/2)\begin{bmatrix}\mathbf{R}_0''(b)-\nu b^{-1}\mathbf{R}_0'(b)\\ \mathbf{R}'''_0(b)+b^{-1}\mathbf{R}_0''(b)-b^{-2}\mathbf{R}_0'(b)\\ \mathbf{R}_0'(a)\\ \mathbf{R}_0'(a)-a^{-1}\mathbf{R}_0(a)\end{bmatrix}^{-1}\begin{bmatrix}\overline{R}_s(b)/\omega_s\\ \overline{R}_s'(b)/\omega_s\\ 0\\ 0\end{bmatrix} \tag{B.9}$$

As a result, the homogenous solution is obtained,

$$\Psi_H=[\,1 \quad r^2 \quad \ln r \quad r^2\ln r\,]\mathbf{c}_0^H \tag{B.10}$$

Appendix C. Formula derivations of the non-homogenous solution Ψ_N

The non-homogenous form of Eqs. (16)–(18) can be written as

$$\nabla^4\Psi_N = -E\alpha_T\nabla^2 I_\Theta = -2E\alpha_T\Theta_D\sum_{s=1}^{\infty}\omega_s\overline{R}_s(r)\sin(\omega_s h/2) \tag{C.1}$$

$$\left[\frac{\partial^2\Psi_N}{\partial r^2}-\nu\left(\frac{1}{r}\frac{\partial\Psi_N}{\partial r}+\frac{1}{r^2}\frac{\partial^2\Psi_N}{\partial\theta^2}\right)\right]\Bigg|_{r=b}=0, \quad \left[\frac{\partial}{\partial r}(\nabla^2\Psi_N)+\frac{1+\nu}{r^2}\frac{\partial^2}{\partial\theta^2}\left(\frac{\partial\Psi_N}{\partial r}-\frac{\Psi_N}{r}\right)\right]\Bigg|_{r=b}=0 \tag{C.2}$$

$$\left(\frac{\partial\Psi_N}{\partial r}+\frac{1}{r}\frac{\partial^2\Psi_N}{\partial\theta^2}\right)\Bigg|_{r=a}=0, \quad \left(\frac{\partial^2\Psi_N}{\partial r\,\partial\theta}-\frac{1}{r}\frac{\partial\Psi_N}{\partial\theta}\right)\Bigg|_{r=a}=0 \tag{C.3}$$

The solution of $\partial^2\Psi_N/\partial t^2+\nabla^4\Psi_N=0$ can be expressed as

$$\Psi_N=\sum_{m=0}^{\infty}\sum_{n=-\infty}^{\infty}\mathrm{e}^{\mathrm{i}n\theta}\mathbf{S}_{m,n}(\gamma_{m,n}r)\mathbf{d}_{m,n}y_{m,n}^N \tag{C.4}$$

where ${y_{m,-n}}^N=\mathrm{conj}({y_{m,n}}^N)$; $\mathbf{S}_{m,n}(\gamma_{m,n}r)=[\,\mathrm{J}_n(\gamma_{m,n}r) \quad \mathrm{Y}_n(\gamma_{m,n}r) \quad \mathrm{I}_n(\gamma_{m,n}r) \quad \mathrm{K}_n(\gamma_{m,n}r)\,]$, $\mathbf{d}_{m,n}=[\,d_1 \quad d_2 \quad d_3 \quad d_4\,]^{\mathrm{T}}$, and $\mathbf{S}_{m,n}(\gamma_{m,n}r)\mathbf{d}_{m,n}=\mathbf{S}_{m,-n}(\gamma_{m,-n}r)\mathbf{d}_{m,-n}$. $\gamma_{m,n}$ and $\mathbf{d}_{m,n}$ can be determined by the self-adjoint eigenvalue problem corresponding to the boundary conditions Eqs. (C.2) and (C.3).

From Galerkin's method, substituting Eq. (C.4) into Eq. (C.1) yields an expression, multiplying the expression by $\mathrm{e}^{-\mathrm{i}n\theta}\mathbf{S}_{m,n}(\gamma_{m,n}r)\mathbf{d}_{m,n}$ and integrating it over the disk area yield ${y_{m,n}}^N=0$ when $n\neq0$. However, when $n=0$, employing the same remaining in Appendix B to the second boundary condition in Eq. (C.3), ${y_{m,0}}^N$ can be solved as

$$y_{m,0}^N=-E\alpha_T\Theta_D\gamma_{m,0}^{-4}\sum_{s=1}^{\infty}2\omega_s\sin(\omega_s h/2)\int_b^a\overline{R}_s(r)\mathbf{S}_{m,0}(\gamma_{m,0}r)\mathbf{d}_{m,0}r\,\mathrm{d}r \tag{C.5}$$

As a result, the non-homogenous solution is obtained,

$$\Psi_N=\sum_{m=0}^{\infty}\mathbf{S}_{m,0}(\gamma_{m,0}r)\mathbf{d}_{m,0}y_{m,0}^N \tag{C.6}$$

Appendix D. Matrices for n nodal diameters

Stiffness matrix for n nodal diameters can be obtained as a diagonal matrix,

$$\mathbf{S}_n=\mathrm{diag}[\,\cdots \quad \Omega_{m,n}^2 \quad \cdots\,] \tag{D.1}$$

where $\Omega_{m,n}=h\kappa_{m,n}^2\sqrt{E/12/\rho/(1-\nu^2)}$, and $\mathbf{S}_n=\mathbf{S}_{-n}$. Moreover, $\mathbf{I}$ is the identity matrix with the same size of $\mathbf{S}_n$.

The matrix induced by membrane stress resultants σ_r, σ_θ of disk rotation can be expressed as

$$\mathbf{L}_n=\begin{bmatrix}\ddots & \vdots & \iddots\\ \cdots & k_{m_1,m_2}^n & \cdots\\ \iddots & \vdots & \ddots\end{bmatrix} \tag{D.2}$$

where $k_{m_1,m_2}^n=a^2\mathbf{c}_{m_1,n}^{\mathrm{T}}[\int_b^a(\sigma_r\mathbf{B}'^{\mathrm{T}}_{m_1,n}\mathbf{B}'_{m_2,n}+\sigma_\theta n^2r^{-2}\mathbf{B}_{m_1,n}^{\mathrm{T}}\mathbf{B}_{m_2,n})r\,\mathrm{d}r]\mathbf{c}_{m_2,n}$, $k_{m_1,m_2}^n=k_{m_2,m_1}^n$, $m_1,m_2=0,1,\ldots,N_m$, and $\mathbf{L}_n=\mathbf{L}_{-n}$.

The matrix induced by thermal stress Ψ can be expressed as

$$\mathbf{R}_n = \begin{bmatrix} \ddots & \vdots & \iddots \\ \cdots & R^n_{m_1,m_2} & \cdots \\ \iddots & \vdots & \ddots \end{bmatrix} \tag{D.3}$$

where $R^n_{m_1,m_2} = (E/\rho h)\mathbf{c}^{\mathrm{T}}_{m_1,n}[\int_b^a(\xi_r \mathbf{B}'^{\mathrm{T}}_{m_1,n}\mathbf{B}'_{m_2,n} + \xi_\theta n^2 r^{-2}\mathbf{B}^{\mathrm{T}}_{m_1,n}\mathbf{B}_{m_2,n})r\,\mathrm{d}r]\mathbf{c}_{m_2,n}$, $R^n_{m_1,m_2} = R^n_{m_2,m_1}$, and $\mathbf{R}_n = \mathbf{R}_{-n}$.

References

[1] L.T. Nieh, C.D. Mote, Vibration and stability in thermally stressed rotating disks, *Experimental Mechanics* 15 (7) (1975) 258–264.
[2] C.D. Mote, A. Rahimi, Real time vibration control of rotating circular plates by temperature control and system identification, *Transactions of the ASME Journal of Dynamic Systems, Measurement and Control* 106 (2) (1984) 123–128.
[3] N.C. Ghosh, Thermal effect on the transverse vibration of high speed rotating anisotropic disk, *Transactions of the ASME Journal of Applied Mechanics* 52 (3) (1985) 543–548.
[4] N. Saniei, A.C.J. Luo, Thermally induced, nonlinear vibrations of rotating disks, *Nonlinear Dynamics* 26 (4) (2001) 393–409.
[5] C. Krempaszky, H. Lippmann, Frictionally excited thermoelastic instabilities of annular plates under thermal pre-stress, *Transactions of the ASME Journal of Tribology* 127 (4) (2005) 756–765.
[6] A.H. Nayfeh, W. Faris, Thermally induced principal parametric resonance in circular plates, *Shock and Vibration* 9 (3) (2002) 143–150.
[7] Y.X. Sun, H. Tohmyoh, Thermoelastic damping of the axisymmetric vibration of circular plate resonators, *Journal of Sound and Vibration* 319 (1-2) (2009) 392–405.
[8] H.N. Arafat, A.H. Nayfeh, W. Faris, Natural frequencies of heated annular and circular plates, *International Journal of Solids and Structures* 41 (11–12) (2004) 3031–3051.
[9] S.A.H. Kordkheili, R. Naghdabadi, Thermoelastic analysis of a functionally graded rotating disk, *Composite Structures* 79 (4) (2007) 508–516.
[10] F. Vivio, V. Vullo, Elastic stress analysis of rotating converging conical disks subjected to thermal load and having variable density along the radius, *International Journal of Solids and Structures* 44 (24) (2007) 7767–7784.
[11] V. Vullo, F. Vivio, Elastic stress analysis of non-linear variable thickness rotating disks subjected to thermal load and having variable density along the radius, *International Journal of Solids and Structures* 45 (20) (2008) 5337–5355.
[12] A.H. Nayfeh, *Non-linear Interactions: Analytical, Computational and Experimental Methods*, Wiley-Interscience, New York, 2000.
[13] J. Awrejcewicz, V.A. Krysko, A.V. Krysko, *Thermo-Dynamics of Plates and Shells*, Springer-Verlag, Berlin, Heidelberg, 2007.
[14] J. Nowinski, *Theory of Thermoelasticity with Applications*, Sijthoff and Noordhff International Publishers, Alphen Aan Den Rijh, 1978.
[15] C. Cho, S. Ahn, Transient thermoelastic analysis of disk brake using the fast Fourier transform and finite element method, *Journal of Thermal Stresses* 25 (3) (2002) 215–243.
[16] A.A. Renshaw, C.D. Mote, Absence of one nodal diameter critical speed modes in an axisymmetric rotating disk, *Transactions of the ASME Journal of Applied Mechanics* 59 (3) (1992) 687–688.